Bioconjugate Chemistry

Article

pubs.acs.org/bc

In Vivo Imaging of Intraperitoneally Disseminated Tumors in Model Mice by Using Activatable Fluorescent Small-Molecular Probes for Activity of Cathepsins

Tomohiko Fujii,[†] Mako Kamiya,[†] and Yasuteru Urano*[,†,‡,§]

[†]Graduate School of Medicine and [‡]Graduate School of Pharmaceutical Sciences, The University of Tokyo, 7-3-1 Hongo, Bunkyo-ku, Tokyo 113-0033, Japan

[§]Basic Research Program, Japan Science and Technology Agency, K's Gobancho, 7, Gobancho, Chiyoda-ku, Tokyo 102-0076, Japan

Supporting Information

ABSTRACT: It is difficult to completely remove carcinomas in unguided ablative surgery because they cannot be distinguished with the unaided human eye. Therefore, in order to precisely visualize tiny tumors and the borders between cancerous lesions and normal tissues, we have been developing fluorescence probes activatable only in cancer cells. We previously reported the hydroxymethylrhodamine green (HMRG)-based fluorescence probe gGlu-HMRG for γ-glutamyltransferase (GGT), which is overexpressed in a variety of cancer cells, and we showed that it enables *in vivo* rapid detection of human ovarian cancer SHIN-3 nodules with a high tumor-to-background (T/B) fluorescence ratio in model mice. However, cancer cell lines with low GGT expression could hardly be detected with gGlu-HMRG. Here we developed two new HMRG-based fluorescence probes for the cathepsin family of cysteine proteases, including cathepsin B (CatB) and cathepsin L (CatL), which show increased expression and/or activity, secretion, and altered localization in many kinds of cancer cells. The developed probes, Z-Phe-Arg-HMRG and Z-Arg-Arg-HMRG, are colorless and nonfluorescent at the physiological pH of 7.4, but are hydrolyzed to HMRG upon reaction with purified cathepsins, resulting in a more than 200-fold fluorescence increase. These probes could visualize human ovarian cancer cell lines SHIN-3, SK-OV-3, and OVCAR-3, of which the latter two were hardly detectable with gGlu-HMRG. Z-Phe-Arg-HMRG showed higher applicability than Z-Arg-Arg-HMRG for *in vivo* imaging, and we confirmed that 0.5-mm-sized SK-OV-3 tumor nodules disseminated on the mesentery in a mouse model could be rapidly visualized by Z-Phe-Arg-HMRG, with a T/B fluorescence ratio of 4.2. Further, intraperitoneally disseminated tumor could be visualized in real time *in vivo* by fluorescence endoscopy after spraying Z-Phe-Arg-HMRG, with a T/B ratio of 3. In conclusion, our HMRG-based activatable probes targeted to cathepsins have expanded the detectable range of cancers, and appear to be suitable for clinical application.

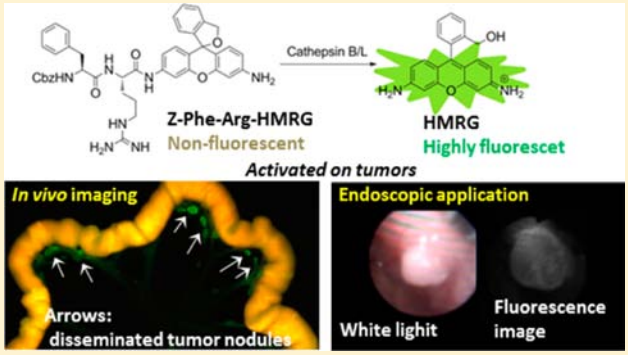

INTRODUCTION

Visualization of cancerous tissues is one of the most important issues in oncotherapeutics. Many difficulties in medical treatment for cancer arise because cancerous tissue cannot be distinguished with the unaided human eye. Several techniques are available to visualize tumors, including MRI, CT scanning, ultrasound imaging, PET (positron emission tomography), and fluorescence imaging.[1] Among them, fluorescence imaging is of particular interest as an aid to guide surgery because of its high sensitivity, high spatial resolution, low cost, portability, simple equipment, rapidity, and absence of ionizing radiation.[2] In particular, the high sensitivity and spatial resolution of fluorescence imaging are favorable for visualizing submillimeter foci in ablative and resectional surgery, making it possible to remove tiny metastatic carcinomas, which are associated with poor prognosis and recurrence of disease. Recently, our group developed an activatable fluorescence probe for γ-glutamyltranspeptidase (GGT),[3] which is overexpressed in a variety of cancer cells. The developed probe, gGlu-HMRG (HMRG: hydroxymethylrhodamine green), is almost completely quenched at the physiological pH of 7.4 due to intramolecular spirocyclization, but is efficiently converted to highly fluorescent HMRG upon reaction with GGT.[3−5] We showed that gGlu-HMRG enables rapid and sensitive *in vivo* imaging of intraperitoneally disseminated tiny tumors in mouse models. However, the applicable range of this probe is limited to GGT-expressing cancers. For example, we could clearly visualize SHIN-3 cells, which have high GGT activitiy,[3] but could not detect SK-OV-3 and OVCAR-3 cells, which have little GGT

Received: July 23, 2014
Revised: August 31, 2014
Published: September 5, 2014

dx.doi.org/10.1021/bc5003289 | *Bioconjugate Chem.* 2014, 25, 1838−1846

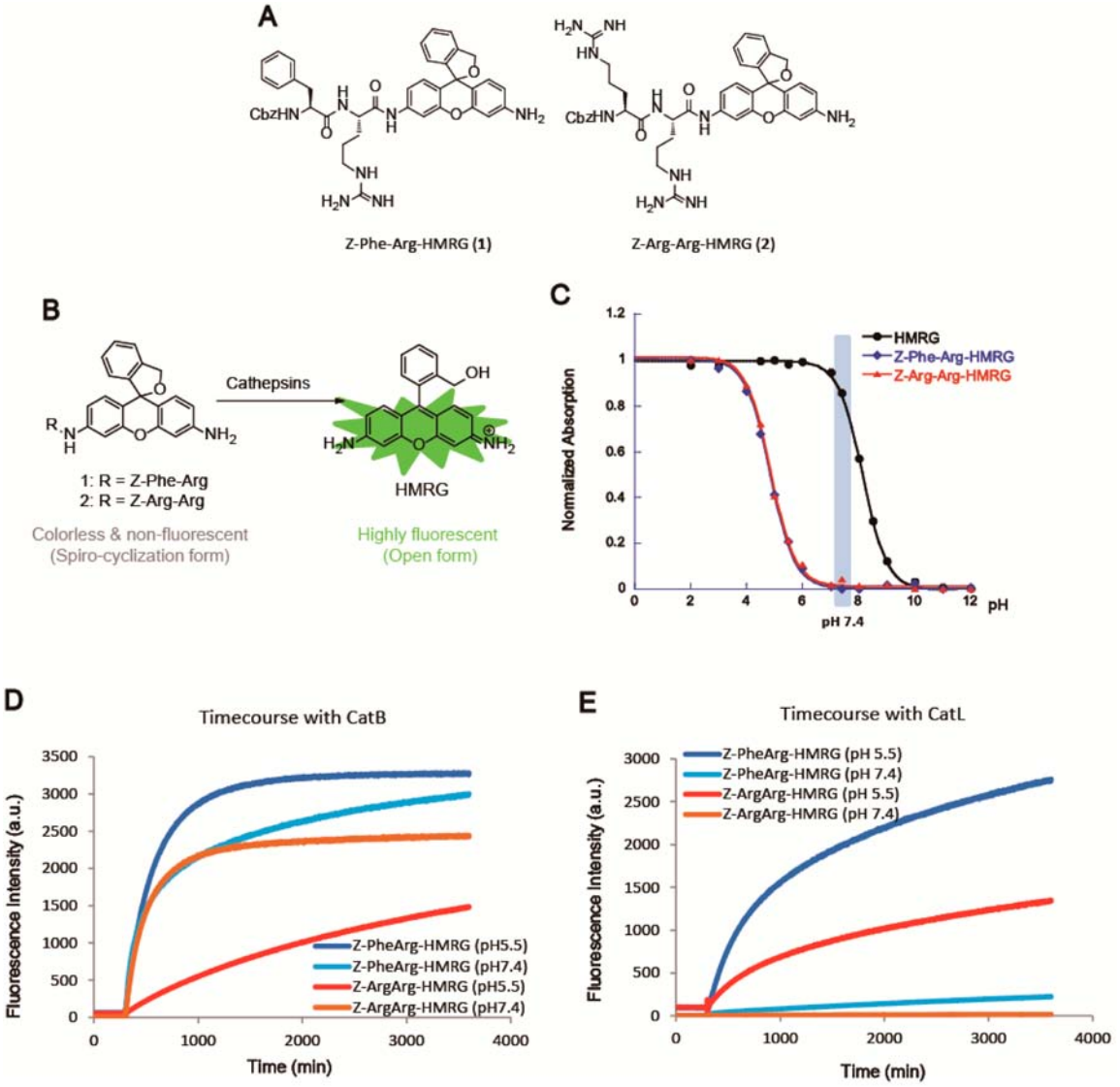

Figure 1. Activatable fluorescence probes for cathepsins based on the HMRG scaffold. (A) Chemical structures of novel cathepsin probes Z-Phe-Arg-HMRG (**1**) and Z-Arg-Arg-HMRG (**2**). (B) Enzymatic reaction of the designed probes with cathepsins. (C) pH-dependency of absorption of HMRG and cathepsin probes. The pK_{cycl} value of cathepsin probes is calculated to be 4.8, so that these probes are nonfluorescent at pH 7.4, whereas the produced HMRG is highly fluorescent at this pH. (D,E) Reactivities of Z-Phe-Arg-HMRG and Z-Arg-Arg-HMRG with cathepsin B at pH 7.4 or 5.5 (D), and with cathepsin L at pH 7.4 or 5.5 (E), at 37 °C.

activity, even though all three cell lines are derived from human ovarian cancer.

In order to extend the range of applicability of HMRG-based fluorescence probes, we aimed to develop new probes targeting other peptidases. For this purpose, we focused on the cathepsin family of cysteine proteases, including cathepsin B[6−9] (CatB) and cathepsin L[10,11] (CatL), which are lysosomal endopeptidases that play various roles in the maintenance of normal cellular metabolism, but show increased expression and/or activity, secretion and change in localization[6,8,12] in breast,[13] colorectal,[14,15] gastric,[16,17] lung,[18] prostate,[19] and ovarian[20−22] carcinomas, gliomas,[23−25] melanomas,[26] and osteoclastoma.[27] CatB and CatL are also known to contribute to the invasion of tumor cells at the basement membrane via degradation of extracellular matrix (ECM) components, including collagen I, collagen IV, laminin, fibronectin, and elastin. Here, we designed and synthesized two fluorescence probes targeted to cathepsins overexpressed in cancers by incorporating enzyme substrate peptides into the HMRG scaffold[28−30] (Figure 1A,B). We examined whether these probes can detect cancer cells with low GGT activity by means of fluorescence imaging studies of cultured cells, spheroids (three-dimensional clusters of cultured cells), and intraperitoneally disseminated tumors in model mice.

RESULTS AND DISCUSSION

Optical Properties of Z-Phe-Arg-HMRG and Z-Arg-Arg-HMRG. First, we examined the optical properties of Z-Phe-Arg-HMRG and Z-Arg-Arg-HMRG. The maximum absorption wavelength ($\lambda_{abs/max}$) was 497 nm, and the maximum emission wavelength ($\lambda_{em/max}$) was 521 nm for both probes. The molar extinction coefficient at pH 7.4 was calculated to be 130 in both cases. The absolute fluorescence quantum yield was 0.38 for Z-Phe-Arg-HMRG, and 0.37 for Z-Arg-Arg-HMRG. The calculated pK_{cycl} value was 4.8 for both probes, and this is sufficiently low that the probe solutions were

dx.doi.org/10.1021/bc5003289 | Bioconjugate Chem. 2014, 25, 1838−1846

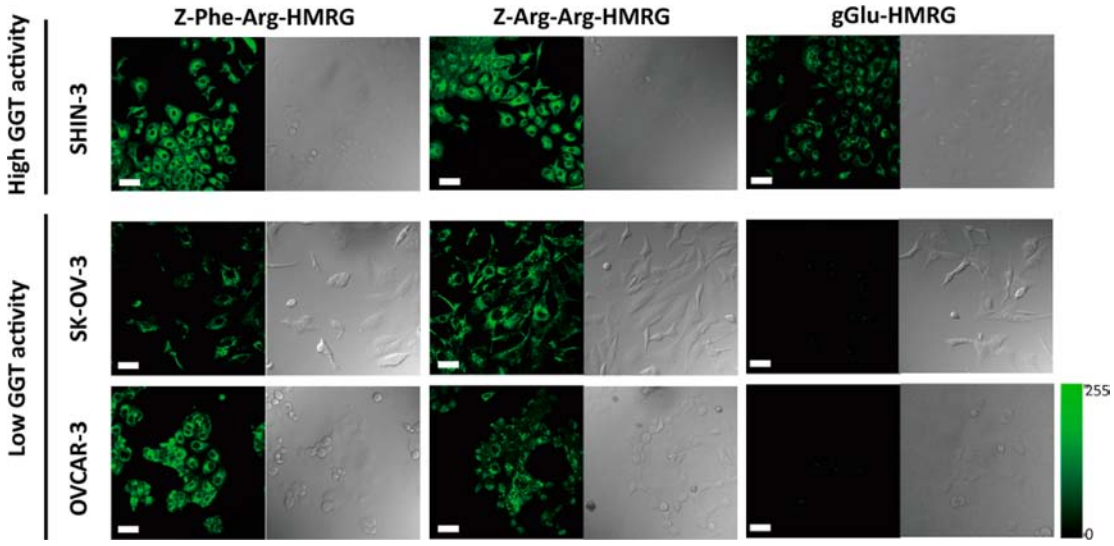

Figure 2. Fluorescence imaging of three cultured cell lines derived from human ovarian cancer cell lines (SHIN-3, SK-OV-3, OVCAR-3) using Z-Phe-Arg-HMRG, Z-Arg-Arg-HMRG, and gGlu-HMRG. Cells were incubated with 1 μM probe solution for 5 min and then images were captured with a Leica TCS SP5X confocal microscopy system (λ_{ex} = 497 nm, λ_{em} = 520 ± 10 nm). Scale bar, 50 μm.

colorless and nonfluorescent at pH 7.4, in contrast to HMRG, the hydrolysis product generated by cathepsin B/L, which is highly fluorescent (its molar extinction coefficient at pH 7.4 is 57000, and its absolute fluorescence quantum yield is 0.81) (Figure 1C). The photochemical properties of the probes compared with those of HMRG are summarized in Supporting Information (Table S1).

***In Vitro* Reaction with Cathepsins.** Next, we examined whether the probes react with cathepsins to produce HMRG by monitoring the fluorescence intensity before and after addition of the enzymes. Cathepsins are normally lysosomal proteases, but it is known that some members of the family, including CatB/L, show altered localization at the cell surface of cancer cells and/or are secreted by cancer cells, serving to degrade ECM components. Therefore, we investigated the reactivities of the probes with these cathepsins not only at pH 5.5 (mimicking the lysosomal pH), but also at pH 7.4 (mimicking the pH at the cell surface). In the reaction of CatB at pH 7.4, a drastic fluorescence increase was observed: an 800-fold increase for Z-Phe-Arg-HMRG and a 200-fold increase for Z-Arg-Arg-HMRG after 1 h reaction (Figure 1D, Supporting Information Figure S1). The *in vitro* conversion of the probe to HMRG by CatB at pH 7.4 was also confirmed by HPLC analysis of reaction solutions (Supporting Information Figure S2). The probes also reacted with CatL at pH 5.5, but hardly reacted with CatL at pH 7.4 (Figure 1E). We also found that Z-Phe-Arg-HMRG showed high reactivity toward cathepsin K,[31] as well as weak reactivity toward cathepsin S,[32] although Z-Arg-Arg-HMRG hardly reacted with either of these enzymes (Supporting Information Figure S3) These results indicate that Z-Phe-Arg-HMRG has relatively broad reactivity toward cathepsin family members, whereas the reactivity of Z-Arg-Arg-HMRG appears to be restricted to CatB/L *in vitro*.

Further, it was confirmed that Z-Phe-Arg-HMRG has higher affinity/reactivity than a commercially available 7-amino-4-methylcoumarin (AMC)-based CatB/L probe toward CatB; K_m and k_{cat} of Z-Phe-Arg-HMRG were calculated to be 30.3 μM and >0.0986 s^{-1} at pH 7.4 at 37 °C with CatB from bovine spleen (Sigma-Aldrich Japan Co., Ltd.) (Supporting Information Table S2), while those of Z-Phe-Arg-MCA[28−30] were calculated to be ≫200 μM and >0.3 s^{-1} under the same conditions. Based on these results, our HMRG-based probe has higher affinity for CatB and is more rapidly hydrolyzed than the AMC-based probe.

Concerning the stability of our cathepsin probes in body fluids, both probes were unstable in mouse blood serum due to the presence of cathepsin activity in serum (Supporting Information Figures S4, S5), indicating that intravenous injection of the probes would not be appropriate. Z-Arg-Arg-HMRG was also unstable in mouse intraperitoneal fluid, which contains a variety of enzyme activity. However, Z-Phe-Arg-HMRG was fairly stable in intraperitoneal fluid, indicating that i.p. injection of Z-Phe-Arg-HMRG is a reasonable approach to visualize tumor nodules disseminated in the peritoneal cavity.

Fluorescence Imaging of Monolayer-Cultured Cell Lines. We then performed fluorescence imaging of cultured human ovarian cancer cell lines having different GGT activities (SHIN-3 with high GGT activity, SK-OV-3 and OVCAR-3 with low GGT activity) with the newly developed probes (Z-Phe-Arg-HMRG and Z-Arg-Arg-HMRG) and our previously developed GGT-activatable probe (gGlu-HMRG). gGlu-HMRG gave a marked fluorescence increase only in GGT-expressing SHIN-3 cells, whereas all three cell lines were clearly visualized with both of the cathepsin probes (Figure 2). Further, in order to examine the enzyme specificity, cultured SK-OV-3 cells were pretreated with cathepsin inhibitor (Z-FF-FMK, permeable: Supporting Information Figure S6) and fluorescence imaging was performed. The fluorescence increase with Z-Phe-Arg-HMRG was strongly suppressed, but that with Z-Arg-Arg-HMRG was not (Figure 3A,B). These results strongly suggested that Z-Phe-Arg-HMRG was activated by cathepsins *in cellulo*, whereas Z-Arg-Arg-HMRG reacted not only with cathepsins, but also with other intracellular hydrolases. Based on these findings together with the results of the stability experiment in intraperitoneal fluid (Supporting Information Figure S4), we selected Z-Phe-Arg-HMRG for *in vivo* imaging using the mouse model.

We also investigated the reaction site of Z-Phe-Arg-HMRG with the enzyme. This probe was activated mainly by intracellular cathepsins to produce HMRG, since HMRG-

dx.doi.org/10.1021/bc5003289 | *Bioconjugate Chem.* 2014, 25, 1838−1846

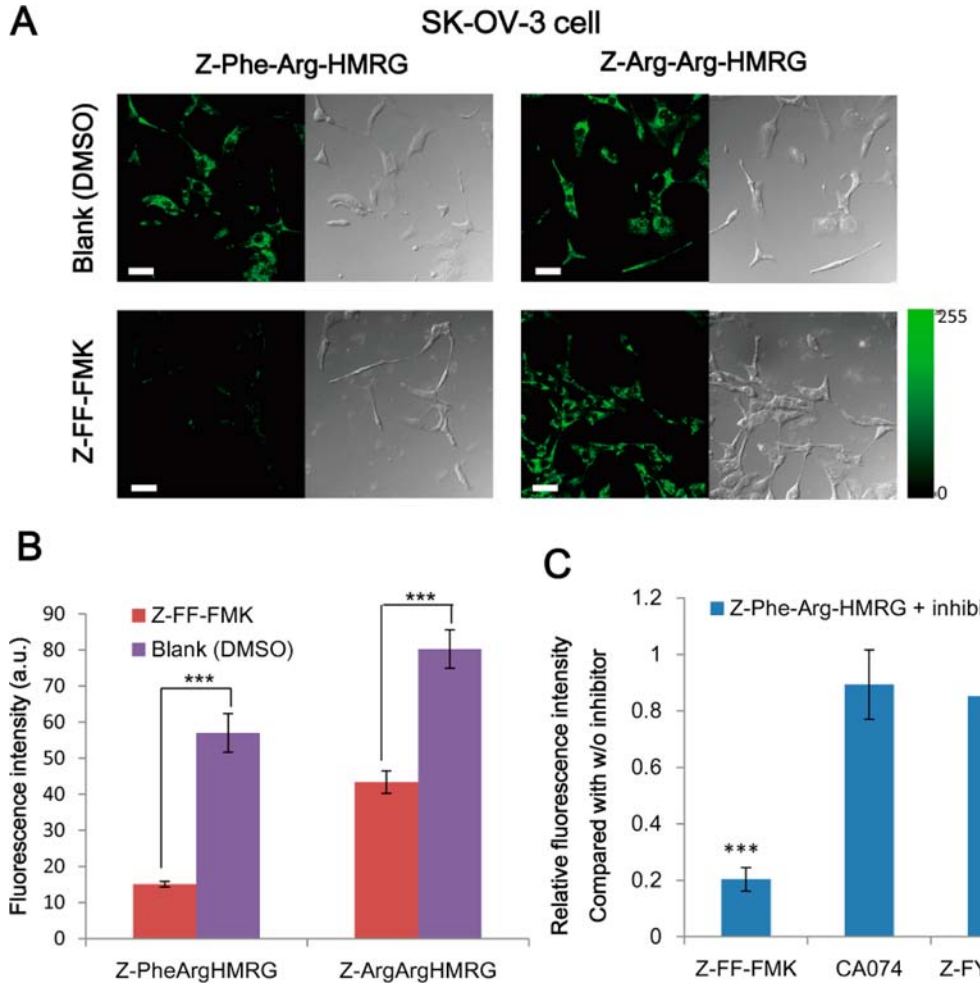

Figure 3. Inhibitory effects of cathepsin inhibitors in SK-OV-3 cell line. (A) Fluorescence imaging of cultured SK-OV-3 cells pretreated with 50 μM Z-FF-FMK (cathepsin inhibitor, cell-permeable) and DMSO as a control. Then, the cells were incubated with 1 μM probe solution, and images were captured with a Leica TCS SP5X confocal microscopy system (λ_{ex} = 497 nm, λ_{em} = 520 ± 10 nm). Scale bar, 50 μm. (B) Quantitative evaluation of ROI fluorescence in SK-OV-3 treated with Z-FF-FMK and DMSO. Error bars represent ± SEM ***P < 0.005. (C) Quantitative evaluation of ROI fluorescence in SK-OV-3 treated with cathepsin inhibitors; Z-FF-FMK (inhibitor for cathepsins, cell-permeable, N = 3, n = 45), CA074 (selective inhibitor for cathepsin B, cell-impermeable, N = 4, n = 60), and Z-FY-CHO (selective inhibitor for cathepsin L, cell-impermeable, N = 3, n = 45). Error bars represent ± SEM. ***P < 0.005.

signals was observed in SK-OV-3 cells even when cell-surface cathepsin activity was inhibited by cell-impermeable inhibitors (CA074, CatB-selective impermeable inhibitor (N = 4, n = 60) and Z-FY-CHO, CatL-selective impermeable inhibitor (N = 3, n = 45)) (Figure 3, Supporting Information Figure S7). In any case, extracellular CatL would not have been involved in hydrolysis of the probe, because it is inactive at pH 7.4 (Figure 1E). Although fluorescence signals may be generated in nontumor tissue due to the intrinsic activity of lysosomal cathepsins, as described later, the tumor-to-background ratio was sufficiently high (3−4-fold) to distinguish tumors in *ex/in vivo* imaging.

Fluorescence Imaging of Cultured Spheroids of SK-OV-3. Compared to two-dimensional monolayer cultures, spheroids may better represent the microenvironment of actual tumor nodules. In order to confirm that cathepsin activities in monolayer cultures are retained in spheroids, we prepared SK-OV-3 spheroids and performed fluorescence imaging with the cathepsin probes. The results were similar to those in monolayer cells (Figure 4), suggesting that the cathepsin activities in monolayer-cultured cells are similar to those in spheroids.

***Ex Vivo* Imaging of Intraperitoneally Disseminated SK-OV-3 Cells in a Mouse Model with Z-Phe-Arg-HMRG.** The SK-OV-3 nude mouse model shows consistent growth of implants in the peritoneal space, similar to the nodules seen in ovarian cancer patients. To investigate whether peritoneal SK-OV-3 ovarian cancer nodules can be detected with Z-Phe-Arg-HMRG in this model, we performed fluorescence imaging 10 min after intraperitoneal injection of the probe. As a control, gGlu-HMRG was similarly applied. Pseudo real color images of normal SK-OV-3 nodules treated with 50 μM Z-Phe-Arg-HMRG are shown in Figure 5A, in which the HMRG fluorescence signal is shown in green pseudo color. Intraperitoneally disseminated SK-OV-3 tumor nodules were clearly visualized with Z-Phe-Arg-HMRG, but not with gGlu-HMRG. In order to confirm that the fluorescent spots observed in Figure 5A represent tumors, we also prepared a mouse model with SK-OV-3/RFP and examined whether the fluorescence signal of Z-Phe-Arg-HMRG coincides with that of RFP (Figure

dx.doi.org/10.1021/bc5003289 | *Bioconjugate Chem.* 2014, 25, 1838−1846

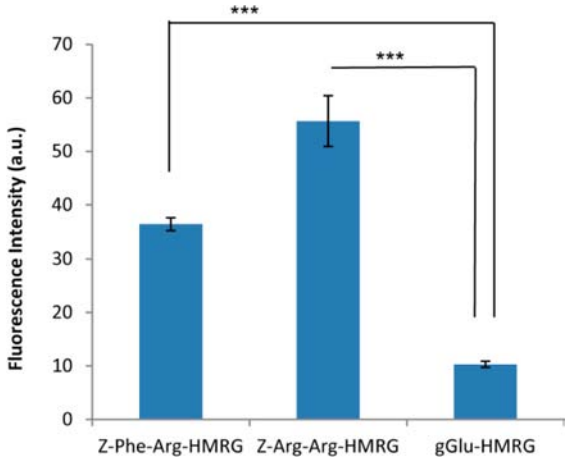

Figure 4. Quantitative evaluation of ROI fluorescence intensity on the surface of SK-OV-3 spheroids treated with 1 μM Z-Phe-Arg-HMRG, 1 μM Z-Arg-Arg-HMRG, and 1 μM gGlu-HMRG (GGT-activatable probe) for 30 min. Error bars represent ± SEM, n = 3−4, respectively.

5B). The results indicate that HMRG reliably detects almost all cancerous tissues on the mesentery.

We further evaluated the T/B ratio of the fluorescence signal by comparing the fluorescence intensity at tumor nodules and at adjacent noncancerous areas on the bowel. The T/B ratio obtained with Z-Phe-Arg-HMRG was 4.2 (Figure 5C), whereas that with gGlu-HMRG was 0.72. The T/B ratio with Z-Phe-Arg-HMRG is sufficiently high to distinguish tumor nodules from normal tissue, presumably reflecting the difference in total cathepsin activity between normal and cancerous tissues. Therefore, we considered that Z-Phe-Arg-HMRG is potentially suitable for clinical application.

Further, in order to confirm that Z-Phe-Arg-HMRG reacts mainly with cathepsins to produce HMRG *in vivo*, we carried out an *ex vivo* experiment with cathepsin inhibitor, Z-FF-FMK (Supporting Information Figure S8). Fluorescence increase at tumor sites was suppressed by the inhibitor, which clearly indicates that the green fluorescence signals were due to HMRG generated by the activity of tumor cathepsins, and were not due to accumulation of Z-Phe-Arg-HMRG itself in cancer cells.

Several activatable fluorescence probes for cathepsin have been reported for tumor imaging. For example, the ProSense series (PerkinElmer Inc.) are commercially available NIR fluorescence probes for cathepsin B/L/S/K activity,[33−36] and have been utilized for *in vivo* imaging of tumors. However, their activation often requires hours to days, which would limit their practical utility for clinical application.[35] Bogyo and coauthors have developed fluorophore-labeled quenching activity-based probes (qABPs) for the cathepsin family,[36−38] and applied these probes for *in vivo* cancer imaging. Although qABPs have the great advantage that they bind covalently to the active site of cysteine cathepsins, these probes also require 30 min to a few hours[39] to generate a sufficient fluorescence signal after injection into mice via the tail vein. Compared to qABPs probes, standard fluorophore-based activatable probes for cathepsin would have the substantial advantage that the fluorescence signal is amplified by enzymatic turnover. Indeed, Z-Phe-Arg-HMRG enabled us to detect carcinoma lesions within only 10 min.

***In Vivo* Fluorescence Endoscopic Study.** In order to simulate the clinical surgical situation, we performed fluorescence imaging by means of endoscopy in the intraperitoneally disseminated SK-OV-3/RFP tumor model. Z-Phe-Arg-HMRG was sprayed onto tumor nodules on the abdomen wall through an endoscopic spray catheter. Fluorescence signals at lesions were observed after 10 min (Figure 6, n = 3). These results show that Z-Phe-Arg-HMRG was activated at tumor sites in vivo within 10 min, with a T/B ratio of 3.

■ CONCLUSION

We have developed a new activatable probe, Z-Phe-Arg-HMRG, targeting cathepsins, and showed that it can detect disseminated tiny tumors in the abdominal cavity of model mice that were undetectable with our previously reported gGlu-HMRG, which targets γ-glutamyltransferase. In other words, we have extended the detectable range of cancers by developing a new activatable probe targeted to other peptidases that are overexpressed in cancer cells. Z-Phe-Arg-HMRG showed very rapid fluorescence activation at tumor sites with a high tumor-to-background fluorescence ratio *in vivo*, and we were able to detect the locations of submillimeter-size tumors within 10 min through a fluorescence endoscopic system simply by spraying the probe onto the target area. Preclinical studies of this probe are already in progress.

■ MATERIALS AND METHODS

Organic Synthesis. Cathepsin probes, Z-Phe-Arg-HMRG (**1**) and Z-Arg-Arg-HMRG (**2**) (Figure 1A), were synthesized according to scheme S1 in the Supporting Information. Synthetic procedures and physical data are also presented in Supporting Information. The purified probes were prepared as 10 mM stock solutions in DMSO and stored at −20 °C.

Equipment and Materials for Optical Properties. All absorbance spectra were recorded with a UV-2450 UV−vis spectrophotometer (Shimadzu Co., Ltd.) and all fluorescence spectra were recorded with an F-7000 fluorescence spectrophotometer (Hitachi Co., Ltd.). Quantum yield was recorded with a Quantaurus-QY absolute PL quantum yield spectrometer (Hamamatsu Co., Ltd.). Purified and activated cathepsin B from bovine spleen (catalog no. C6286, E.C. 3.4.22.1) and cathepsin L from human liver (C6854, E.C. 3.4.22.15) were purchased from Sigma-Aldrich Japan Co., Ltd.

pK_{cycl} Calculation. The equilibrium constant of a compound (pK_{cycl}) was calculated by fitting the pH profile of normalized absorbance at $\lambda_{abs/max}$ (497 nm) with the well-known Henderson−Hasselbalch equation, as described in the previous report.[5]

***In Vitro* Reactivity for Cathepsin B/L.** 3 μM Z-Phe-Arg-HMRG and 3 μM Z-Arg-Arg-HMRG solutions in 0.2 M phosphate buffer at pH 7.4 or 5.5 were prepared. Each solution was warmed to 37 °C with stirring, and 1 U of CatB was added after 5 min. Change in fluorescence intensity was monitored over 1 h (excitation/emission, 497/520 nm). The same procedure was carried out with 4 mU of CatL.

Cell Culture. Three established human ovarian cancer cell lines (SHIN-3[40] provided by Prof. H. Kobayashi, NIH, U.S.A., and SK-OV-3[41] and OVCAR-3[42] purchased from American Type Culture Collection) were used for *in vitro* fluorescence microscopy studies. Cells were grown in culture medium at 37 °C in humidified air containing 5% CO_2. SHIN-3 was grown in RPMI 1640 (Invitrogen) containing 10% fetal bovine serum (FBS, Invitrogen), 0.03% L-glutamine, and PS (100 U/mL penicillin and 100 μg/mL streptomycin). OVCAR-3 was grown

dx.doi.org/10.1021/bc5003289 | *Bioconjugate Chem.* 2014, 25, 1838−1846

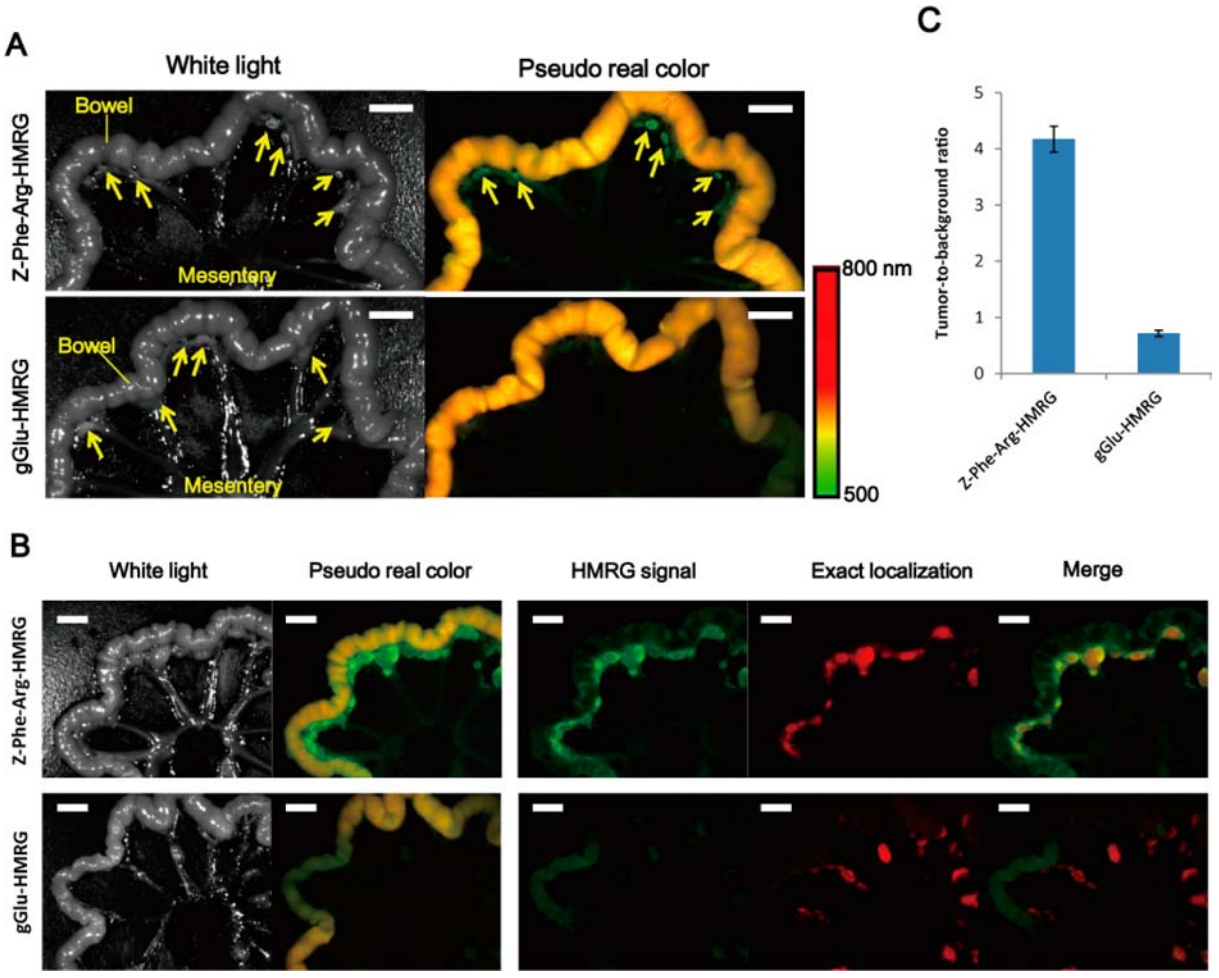

Figure 5. *Ex vivo* imaging of SK-OV-3 disseminated model mice treated with HMRG-based probes. (A) White light (left) and pseudo real color images (right) obtained with a 465/30 nm band-pass filter for excitation and a 515 nm long-pass filter for emission. The mesentery from SK-OV-3 disseminated model mouse preincubated with 50 μM Z-Phe-Arg-HMRG or gGlu-HMRG for 10 min was spread and imaged with a Maestro In-Vivo imaging system. Green color indicates the HMRG signal and orange color corresponds to autofluorescence from digested material in the bowel. Yellow arrows indicate tumor locations confirmed with the naked eye. Scale bars represent 5.0 mm. (B) White light, pseudo real color, unmixed spectra image (green, HMRG signals; red, RFP signals), and merged image of spread mesentery of SK-OV-3/RFP disseminated model mice treated with HMRG probes. Scale bars represent 5.0 mm. (C) Quantitative evaluation of the fluorescence signal at SK-OV-3/RFP nodules on the mesentery. Compared with adjacent noncancerous areas on the bowel, fluorescence on tumors showed 4.2-fold greater intensity with Z-Phe-Arg-HMRG. Error bars represent ± SEM; N = 4, n = 38 with Z-Phe-Arg-HMRG; N = 3, n = 17 with gGlu-HMRG.

in RPMI 1640 containing 20% FBS, 0.03% L-glutamine, and PS. SK-OV-3 was grown in McCoy's 5A (Invitrogen) containing 10% FBS, 0.03% L-glutamine, and PS.

Fluorescence Microscopy of Monolayer-Cultured Cell Lines. For fluorescence microscopy, about 10 000 cells were seeded in each partition of an 8-well chamber (μ-Slide 8 well; Ibidi) and incubated at 37 °C, in atmosphere of 5% CO_2, for 24 h. The medium was removed and the cells were washed with Hank's Balanced Salt Solution (HBSS) and incubated with Z-Phe-Arg-HMRG or Z-Arg-Arg-HMRG or gGlu-HMRG (final concentration 1 μM) in HBSS for 5 min. Fluorescence images were captured with a Leica Application Suite Advanced Fluorescence (LAS-AF) microscope with a TCS SP5 unit equipped with a 60× objective lens (excitation/emission, 497/515−535 nm).

Inhibitory Assay. Z-FF-FMK (permeable cathepsin inhibitor),[43−45] CA074 (impermeable CatB inhibitor),[46−49] and Z-FY-CHO (impermeable CatL inhibitor)[50,51] were purchased from Calbiochem (Merck Co., Ltd.) and used at 50 μM final concentration. After preincubation of inhibitor solution in HBSS (final concentration: 50 μM) for 5 min, the cultured SK-OV-3 cells were incubated for 5 min with Z-Phe-Arg-HMRG and Z-Arg-Arg-HMRG (final concentration: 1 μM) and fluorescence images were captured with the LAS-AF microscope as described above.

Preparation of SK-OV-3 Spheroids.[52] A round-bottomed 96-well plate for cell culture was precoated with 50 μL of 0.5% poly-HEMA (poly 2-hydroxyethyl methacrylate; Sigma, P3932) in 95% ethanol and air-dried at room temperature overnight. 5000 to 10 000 SK-OV-3 cells in 5% Matrigel were placed in each well. The plate was centrifuged at 1000g for 10 min, and incubated at 37 °C under an atmosphere of 5% CO_2 for 7 days. The cells formed three-dimensional clusters with diameters of 300−400 μm.

Fluorescence Imaging of Spheroids of SK-OV-3. Fluorescence imaging of SK-OV-3 spheroids was performed with Z-Phe-Arg-HMRG and Z-Arg-Arg-HMRG, with gGlu-HMRG as a control. Spheroids cultured for 7 days on round-bottomed wells coated with poly-HEMA were transferred to an 8-well chamber, and then incubated with Z-Phe-Arg-HMRG

dx.doi.org/10.1021/bc5003289 | *Bioconjugate Chem.* 2014, 25, 1838−1846

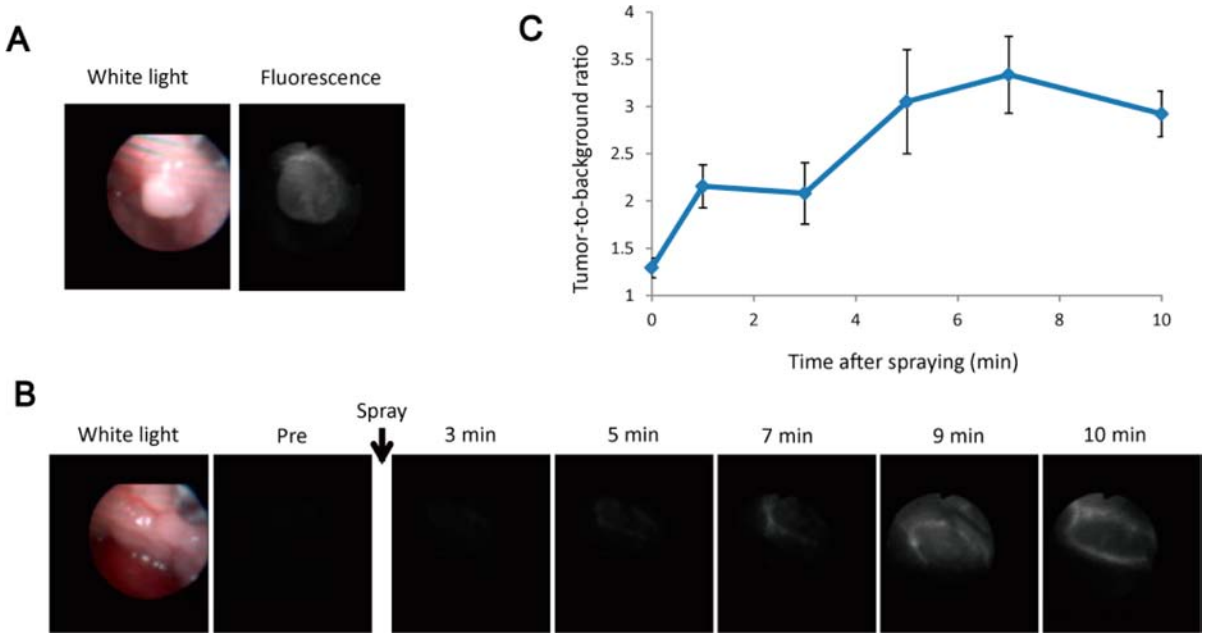

Figure 6. Pictures obtained with an endoscopic imaging system. (A) SK-OV-3/RFP tumors on the peritoneal wall of model mice preinjected with Z-Phe-Arg-HMRG 10 min before imaging. Fluorescence images were obtained through excitation and emission filters of 465 to 500 nm and 516 to 556 nm, respectively. (B) Sequential fluorescence images of the cancerous area over 10 min, starting from just after spraying with 50 μM Z-Phe-Arg-HMRG. (C) Changes in tumor-to-background (T/B) ratio. Error bars represent ± SEM, n = 3.

and Z-Arg-Arg-HMRG (final concentration: 1 μM) in HBSS for 30 min in 37 °C. Fluorescence images were captured with an LAS-AF microscope as described above. ROIs were drawn within the spheroid surface, and the fluorescence intensity on each ROI was averaged (n = 3−4) and normalized with respect to ROI fluorescence on spheroids treated with 1 μM HMRG.

Preparation of Intraperitoneal Tumor-Bearing Model Mice. All experimental protocols were in accordance with the policies of the Animal Ethics Committee of the University of Tokyo. Human ovarian cancer cell lines, SK-OV-3 and SK-OV-3/RFP (Cell Biolabs, Inc.), were implanted by intraperitoneal injection of 5×10^6 to 1×10^7 cells suspended in 300 to 400 μL of PBS into female nude mice (BALB/cA Jcl-*nu/nu*, Clea Japan Inc.). Experiments with tumor-bearing mice were performed after 10 and 20 days, when disseminated peritoneal implants had reached about 0.5−3 mm in size.

***Ex Vivo* Fluorescence Imaging.** A 50 μM solution of Z-Phe-Arg-HMRG in 300 μL PBS was injected intraperitoneally into the abdominal cavity of SK-OV-3 model mice. After 10 min incubation, the mice were killed with CO_2 and the abdominal cavity was exposed. Fluorescence images were obtained with the Maestro In-Vivo imaging system (PerkinElmer Inc.) equipped with a 465/30 nm band-pass filter for excitation and a 515 nm long-pass filter for emission. The tunable filter was automatically stepped in 10 nm increments from 500 to 800 nm, and images at each wavelength corresponding to each pseudo color were integrated to obtain pseudo real color images. Fluorescence images consisting of the spectra of HMRG and autofluorescence derived from digested pelleted feed were also obtained as pseudo real color images.

In order to check the locations of disseminated tumors on the mesentery, SK-OV-3 cells stably expressing RFP (SK-OV-3/RFP) was also subjected to the above procedure. Fluorescence images of RFP spectra were obtained using a 570/40 nm band-pass filter for excitation and a 630 nm long-pass filter for emission. Spectral fluorescence images consisting of HMRG and RFP spectral signals were left unmixed by the Maestro software and were merged to confirm the precise locations of tumors.

Tumor-to-background (T/B) ratio was also calculated. ROIs were drawn within the tumors confirmed by RFP signals and adjacent noncancerous areas. The average fluorescence intensity of each ROI was calculated by Maestro software. The number of ROIs placed in the tumor nodules was 38 for Z-Phe-Arg-HMRG, and 17 for gGlu-HMRG. The same numbers of ROIs were placed in noncancerous areas. The T/B ratio was calculated as the average fluorescence intensity of tumors divided by that of adjacent normal tissue.

***In Vivo* Real-Time Fluorescence Endoscopic Imaging.** A fluorescence endoscopic system (Evis Exera-II XCLV-180, Olympus) equipped with a fiberoptic endoscope (XBF-MP60, Olympus) was used. Excitation and emission filters were 465 to 500 nm and 516 to 556 nm, respectively. Mice were anesthetized by intraperitoneal injection of ketamine−xylazine solution (2 mg ketamine and 0.2 mg xylazine per mouse) and further anesthetized by continuous flow of 0.5−2% isoflurane gas. The endoscope was inserted into the abdominal cavity through a small incision in the lower abdomen, and the abdominal cavity was inflated with air. A 50 μM solution of Z-Phe-Arg-HMRG in 400 μL PBS was sprayed inside the abdominal cavity through the endoscopic spray catheter during video monitoring/recording. The change in fluorescence intensity of the cancerous tissue was monitored for 10 min, and the T/B ratio was calculated.

■ ASSOCIATED CONTENT

Ⓢ Supporting Information

Additional characterization data on the activatable probes for cathepsin activity are presented. This material is available free of charge via the Internet at http://pubs.acs.org.

dx.doi.org/10.1021/bc5003289 | *Bioconjugate Chem.* 2014, 25, 1838−1846

AUTHOR INFORMATION

Corresponding Author

*E-mail: uranokun@m.u-tokyo.ac.jp. Tel: (+81)358413568. Fax: (+81)358413563.

Notes

The authors declare no competing financial interest.

ACKNOWLEDGMENTS

This research was supported in part by the Ministry of Education, Culture, Sports, Science and Technology of Japan (Grant-in-Aid for Scientific Research (KAKENHI), grants 20117003 and 23249004 to Y.U., grants 23113504, 25113707, 25870180 to M.K.), by The Daiichi-Sankyo Foundation of Life Science (grant to Y.U.), by The Mochida Memorial Foundation for Medical and Pharmaceutical Research (grant to M.K.), by The Tokyo Society of Medical Sciences (grant to M.K.). We thank Prof. Hisataka Kobayashi for the kind gift of the SHIN-3 cell line used in this study.

REFERENCES

(1) Frangioni, J. V. (2008) New technologies for human cancer imaging. *J. Clin. Oncol. 26*, 4012−4021.

(2) Weissleder, R., and Pittet, M. J. (2008) Imaging in the era of molecular oncology. *Nature 452*, 580−589.

(3) Urano, Y., Sakabe, M., Kosaka, N., Ogawa, M., Mitsunaga, M., Asanuma, D., Kamiya, M., Young, M. R., Nagano, T., Choyke, P. L., and Kobayashi, H. (2011) Rapid cancer detection by topically spraying a γ-glutamyltranspeptidase-activated fluorescent probe. *Sci. Transl. Med. 3*, 110ra119.

(4) Kobayashi, H., Ogawa, M., Alford, R., Choyke, P. L., and Urano, Y. (2010) New strategies for fluorescent probe design in medical diagnostic imaging. *Chem. Rev. 110*, 2620−2640.

(5) Sakabe, M., Asanuma, D., Kamiya, M., Iwatate, R. J., Hanaoka, K., Terai, T., Nagano, T., and Urano, Y. (2013) Rational design of highly sensitive fluorescence probes for protease and glycosidase based on precisely controlled spirocyclization. *J. Am. Chem. Soc. 135*, 409−414.

(6) Koblinski, J. E., Ahram, M., and Sloane, B. F. (2000) Unraveling the role of proteases in cancer. *Clin. Chim. Acta 291*, 113−135.

(7) Mason, S. D., and Joyce, J. A. (2011) Proteolytic networks in cancer. *Trends Cell Biol. 21*, 228−237.

(8) Podgorski, I., and Sloane, B. F. (2003) Cathepsin B and its role(s) in cancer progression. *Biochem. Soc. Symp. 70*, 263−276.

(9) Gondi, C. S., and Rao, J. S. (2013) Cathepsin B as a cancer target. *Expert Opin. Ther. Targets 17*, 281−291.

(10) Lankelma, J. M., Voorend, D. M., Barwari, T., Koetsveld, J., Van der Spek, A. H., De Porto, A. P., Van Rooijen, G., and Van Noorden, C. J. (2010) Cathepsin L, target in cancer treatment? *Life Sci. 86*, 225−233.

(11) Leto, G., Sepporta, M. V., Crescimanno, M., Flandina, C., and Tumminello, F. M. (2010) Cathepsin L in metastatic bone disease: therapeutic implications. *Biol. Chem. 39*, 655−664.

(12) Mai, J., Waisman, D. M., and Sloane, B. F. (2000) Cell surface complex of cathepsin B/annexin II tetramer in malignant progression. *Biochim. Biophys. Acta 1477*, 215−230.

(13) Bengsch, F., Buck, A., Günther, S. C., Seiz, J. R., Tacke, M., Pfeifer, D., Elverfeldt, D., Sevenich, L., Hillebrand, L. E., Kern, U., Sameni, M., Peters, C., Sloane, B. F., and Reinheckel, T. (2013) Cell type-dependent pathogenic functions of overexpressed human cathepsin B in murine breast cancer progression. *Oncogene*, 1−11.

(14) Jessup, J. M. (1994) Cathepsin B and other proteases in human colorectal carcinoma. *Am. J. Pathol. 145*, 253−262.

(15) Keppler, D., Abrahamson, M., and Sordat, B. (1994) Secretion of cathepsin B and tumour invasion. *Biochem. Soc. Trans. 22*, 43−49.

(16) Ebert, M. P., Krüger, S., Fogeron, M. L., Lamer, S., Chen, J., Pross, M., Schulz, H. U., Lage, H., Heim, S., Roessner, A., Malfertheiner, P., and Röcken, C. (2005) Overexpression of cathepsin B in gastric cancer identified by proteome analysis. *Proteomics 5*, 1693−1704.

(17) Czyzewska, J., Guzińska-Ustymowicz, K., Kemona, A., and Bandurski, R. (2008) The expression of matrix metalloproteinase 9 and cathepsin B in gastric carcinoma is associated with lymph node metastasis,but not with postoperative survival. *Folia Histochem. Cytobiol. 46*, 57−64.

(18) Sukoh, N., Abe, S., Ogura, S., Isobe, H., Takekawa, H., Inoue, K., and Kawakami, Y. (1994) Immunohistochemical study of cathepsin B. Prognostic significance in human lung cancer. *Cancer 74*, 46−51.

(19) Sinha, A. A., Wilson, M. J., Gleason, D. F., Reddy, P. K., Sameni, M., and Sloane, B. F. (1995) Immunohistochemical localization of cathepsin B in neoplastic human prostate. *Prostate 26*, 171−178.

(20) Downs, L. S., Jr., Lima, P. H., Bliss, R. L., and Blomquist, C. H. (2005) Cathepsins B and D activity and activity ratios in normal ovaries, benign ovarian neoplasms, and epithelial ovarian cancer. *J. Soc. Gynecol. Investig. 12*, 539−544.

(21) Nishikawa, H., Ozaki, Y., Nakanishi, T., Blomgren, K., Tada, T., Arakawa, A., and Suzumori, K. (2004) The role of cathepsin B and cystatin C in the mechanisms of invasion by ovarian cancer. *Gynecol. Oncol. 92*, 881−886.

(22) Haczyńksa, H., Gerber, J., Osada, J., and Warwas, M. (1997) The activities and subcellular localization of cathepsin B and cysteine proteinase inhibitors in human ovarian carcinoma. *Acta Biochim. Polym. 44*, 113−120.

(23) Levicar, N., Nuttall, R. K., and Lah, T. T. (2003) Proteases in brain tumour progression. *Acta Neurochir 145*, 825−838.

(24) Mai, J., Sameni, M., Mikkelsen, T., and Sloane, B. F. (2002) Degradation of extracellular matrix protein tenascin-C by cathepsin B: an interaction involved in the progression of gliomas. *Biol. Chem. 383*, 1407−1413.

(25) Rempel, S. A., Rosenblum, M. L., Mikkelsen, T., Yan, P. S., Ellis, K. D., Golembieski, W. A., Sameni, M., Rozhin, J., Ziegler, G., and Sloane, B. F. (1994) Cathepsin B expression and localization in glioma progression and invasion. *Cancer Res. 54*, 6027−6031.

(26) Sloane, B. F., Dunn, J. R., and Honn, K. V. (1981) Lysosomal cathepsin B: correlation with metastatic potential. *Science 212*, 1151−1153.

(27) Page, A. E., Warburton, M. J., Chambers, T. J., Pringle, J. A., and Hayman, A. R. (1992) Human osteoclastomas contain multiple forms of cathepsin B. *Biochim. Biophys. Acta 1116*, 57−66.

(28) Morita, T., Kato, H., Iwanaga, S., Takada, K., and Kimura, T. (1977) New fluorogenic substrates for alpha-thrombin, factor Xa, kallikreins, and urokinase. *J. Biochem. 82*, 1495−1498.

(29) Barrett, A. J. (1980) Fluorimetric assays for cathepsin B and cathepsin H with methylcoumarylamide substrates. *Biochem. J. 187*, 909−912.

(30) Barrett, A. J., and Kirschke, H. (1981) Cathepsin B, cathepsin H, and cathepsin L. *Methods Enzymol. 80*, 535−61.

(31) Novinec, M., and Lenarč ič, B. (2013) Cathepsin K: a unique collagenolytic cysteine peptidase. *Biol. Chem. 394*, 1163−1179.

(32) Wang, B., Sun, J., Kitamoto, S., Yang, M., Grubb, A., Chapman, H. A., Kalluri, R., and Shi, G. P. (2006) Cathepsin S controls angiogenesis and tumor growth via matrix-derived angiogenic factors. *J. Biol. Chem. 281*, 6020−6029.

(33) Weissleder, R., Tung, C., Mahmood, U., and Bogdanov, A., Jr. (1999) In vivo imaging of tumors with proteaseactivated near-infrared fluorescent probes. *Nat. Biotechnol. 17*, 375−378.

(34) Onda, N., Kemmochi, S., Morita, R., Ishihara, Y., and Shibutani, M. (2013) In vivo imaging of tissue-remodeling activity involving infiltration of macrophages by a systemically administered protease-activatable probe in colon cancer tissues. *Translational Oncology 6*, 628−637.

(35) Nahrendorf, M., Sosnovik, D. E., Waterman, P., Swirski, F. K., Pande, A. N., Aikawa, E., Figueiredo, J., Pittet, M. J., and Weissleder, R. (2007) Dual channel optical tomographic imaging of leukocyte recruitment and protease activity in the healing myocardial infarct. *Circ. Res. 100*, 1218−1225.

(36) Blum, G., Degenfeld, G., Merchant, M. J., Blau, H. M., and Bogyo, M. (2007) Noninvasive optical imaging of cysteine protease activity using fluorescently quenched activity-based probes. *Nat. Chem. Biol. 3*, 668−667.
(37) Paulick, M. G., and Bogyo, M. (2011) Development of activity-based probes for cathepsin X. *ACS Chem. Biol. 6*, 563−572.
(38) Edgington, L. E., Verdoes, M., Ortega, A., Withana, N. P., Lee, J., Syed, S., Bachmann, M. H., Blum, G., and Bogyo, M. (2012) Functional imaging of legumain in cancer using a new quenched activity-based probe. *J. Am. Chem. Soc. 135*, 174−182.
(39) Edgington, L. E., and Bogyo, M. (2013) In vivo imaging and biochemical characterization of protease function using fluorescent activity-based probes. *Curr. Protoc. Chem. Biol. 5*, 25−44.
(40) Imai, S., Kiyozuka, Y., Maeda, H., Noda, T., and Hosick, H. L. (1990) Establishment and characterization of a human ovarian serous cystadenocarcinoma cell line that produces the tumor markers CA-125 and tissue polypeptide antigen. *Oncology 47*, 177−184.
(41) Hung, M. C., Zhang, X., Yan, D. H., Zhang, H. Z., He, G. P., Zhang, T. Q., and Shi, D. R. (1992) Aberrant expression of the c-erbB-2/neu protooncogene in ovarian cancer. *Cancer Lett. 61*, 95−103.
(42) Hamilton, T. C., Young, R. C., and Ozols, R. F. (1984) Experimental model systems of ovarian cancer: applications to the design and evaluation of new treatment approaches. *Semin. Oncol. 11*, 285−298.
(43) Ravanko, K., Järvinen, K., Helin, J., Kalkkinen, N., and Hölttä, E. (2004) Cysteine cathepsins are central contributors of invasion by cultured adenosylmethionine decarboxylase-transformed rodent fibroblasts. *Cancer Res. 64*, 8831−8838.
(44) Esser, R. E., Angelo, R. A., Murphey, M. D., Watts, L. M., Thornburg, L. P., Palmer, J. T., Talhouk, J. W., and Smith, R. E. (1994) Cysteine proteinase inhibitors decrease articular cartilage and bone destruction in chronic inflammatory arthritis. *Arthritis Rheum. 37*, 236−247.
(45) Shaw, E., Mohanty, S., Colic, A., Stoka, V., and Turk, V. (1993) The affinity-labelling of cathepsin S with peptidyl diazomethyl ketones. Comparison with the inhibition of cathepsin L and calpain. *FEBS Lett. 334*, 340−342.
(46) Murata, M., Miyashita, S., Yokoo, C., Tamai, M., Hanada, K., Hatayama, K., Towatari, T., Nikawa, T., and Katunuma, N. (1991) Novel epoxysuccinyl peptides. Selective inhibitors of cathepsin B, in vitro. *FEBS Lett. 280*, 307−10.
(47) Steverding, D. (2011) The cathepsin B-Selective inhibitors CA-074 and CA-074Me inactivate cathepsin L under reducing conditions. *Open Enzyme Inhibition Journal 4*, 11−16.
(48) Asai, M., Yagishita, S., Iwata, N., Saido, T. C., Ishiura, S., and Maruyama, K. (2011) An alternative metabolic pathway of amyloid precursor protein C-terminal fragments via cathepsin B in a human neuroglioma model. *FASEB J. 10*, 3720−3730.
(49) Bogyo, M., Verhelst, S., Bellingard-Dubouchaud, V., Toba, S., and Greenbaum, D. (2000) Selective targeting of lysosomal cysteine proteases with radiolabeled electrophilic substrate analogs. *Chem. Biol. 7*, 27−38.
(50) Boudreau, F., Lussier, C. R., Mongrain, S., Darsigny, M., Drouin, J. L., Doyon, G., Suh, E. R., Beaulieu, J. F., Rivard, N., and Perreault, N. (2007) Loss of cathepsin L activity promotes claudin-1 overexpression and intestinal neoplasia. *FASEB J. 21*, 3853−3865.
(51) Chung, J. H., Im, E. K., Jin, T., Lee, S. M., Kim, S. H., Choi, E. Y., Shin, M. J., Lee, K. H., and Jang, Y. (2011) Cathepsin L derived from skeletal muscle cells transfected with bFGF promotes endothelial cell migration. *Exp. Mol. Med. 43*, 179−188.
(52) Ivascu, A., and Kubbies, M. (2006) Rapid generation of single-tumor spheroids for high-throughput cell function and toxicity analysis. *J. Biomol. Screen. 11*, 922−932.